

## RAPID COMMUNICATION

# High-reflectivity GaN/air vertical distributed Bragg reflectors fabricated by wet etching of sacrificial AlInN layers

C Xiong<sup>1</sup>, P R Edwards<sup>2</sup>, G Christmann<sup>3</sup>, E Gu<sup>4</sup>, M D Dawson<sup>4</sup>,  
J J Baumberg<sup>3</sup>, R W Martin<sup>2</sup> and I M Watson<sup>4,5</sup>

<sup>1</sup> School of Physics and State Key Laboratory of Artificial Microstructure and Mesoscopic Physics, Peking University, Beijing 100871, People's Republic of China

<sup>2</sup> Department of Physics, SUPA, University of Strathclyde, Glasgow G4 0NG, UK

<sup>3</sup> Cavendish Laboratory, University of Cambridge, Cambridge CB3 0HE, UK

<sup>4</sup> Institute of Photonics, SUPA, University of Strathclyde, Glasgow G4 0NW, UK

E-mail: [i.m.watson@strath.ac.uk](mailto:i.m.watson@strath.ac.uk)

Received 26 October 2009, in final form 22 December 2009

Published 5 February 2010

Online at [stacks.iop.org/SST/25/032001](http://stacks.iop.org/SST/25/032001)

## Abstract

Microstructures containing GaN/air distributed Bragg reflector (DBR) regions were fabricated by a selective wet etch to remove sacrificial AlInN layers from GaN–AlInN multilayers. The epitaxial multilayers were grown on free-standing GaN substrates, and contained AlInN essentially lattice matched with GaN in order to minimize strain. Two geometries were defined for study by standard lithographic techniques and dry etching: cylindrical pillars and doubly anchored rectangular bridges. Microreflectivity spectra were recorded from the air-gap DBRs, and indicated peak reflectivities exceeding 70% for a typical 3-period microbridge. These values are likely to be limited by the small scale of the features in comparison with the measurement spot. The stopband in this case was centred at 409 nm, and the reflectivity exceeded 90% of the maximum over 73 nm. Simulations of reflectance spectra, including iterations to layer thicknesses, gave insight into the tolerances achievable in processing, in particular indicating bounds on the parasitic removal of GaN layers during wet etching. Air-gap nitride DBRs as described can be further developed in various ways, including adaptation for electrostatic tuning, incorporation into microcavities, and integration with active emitters.

(Some figures in this article are in colour only in the electronic version)

## Introduction

Distributed Bragg reflectors (DBRs) comprising alternate layers of a semiconductor and air offer high reflectivities from very few repeat periods, while electrostatic tuning is also possible in appropriate embodiments. Vertical DBRs can be made from epitaxial heterostructures by a sequence of vertical etching and selective lateral etching, provided that

one of the as-grown materials has appropriate properties to act as a sacrificial layer. Such DBRs are necessarily made as microstructures, because of constraints posed by finite etch rates and mechanical stability of the completed air-gap structure. Examples taking advantage of relatively mature growth and processing include tunable InP-air DBRs for near-infrared telecommunication wavelengths [1–3]. Development of sacrificial layer technologies has proved more challenging for wide bandgap III-nitride semiconductors, and progress to 2007 was covered in an extensive review [4]. The first

<sup>5</sup> Author to whom any correspondence should be addressed.

published examples of vertical air-spaced nitride DBRs used a photoelectrochemical (PEC) selective etch of InGaN-based superlattice layers [5, 6]. New opportunities in the fabrication of nitride-air vertical DBRs, and simpler processing routes, are offered by the ternary alloy AlInN [7–9]. This alloy can be grown lattice matched to GaN, and strain-balanced epitaxial multilayers containing AlInN are competitive with other conventional monolithic nitride DBRs. However, these depend on a refractive index difference of only 0.2 or less between adjacent layers, compared to the difference of  $\sim 1.4$  in GaN-air structures. Cho *et al* reported simulated reflectance spectra for the latter type of structure, showing that peak reflectivities at 450 nm reach essentially 100% with as few as 4 repeat periods [10].

The method of fabricating vertical GaN-air DBRs presented here involved selective wet etching with hot nitric acid of multiple AlInN layers grown close to the lattice-matched composition of  $\text{Al}_{0.17}\text{In}_{0.83}\text{N}$ . Importantly, the AlInN etch does not show pronounced chemical attack on the reactive GaN (000 $\bar{1}$ ) crystal face, which is progressively exposed as the AlInN is removed. We have previously applied similar processing sequences to structures containing single sacrificial AlInN layers, in order to fabricate microbridges and planar microcavities [11–14]. The application of our microfabrication method using lateral etching of AlInN to epitaxial multilayers, and the associated microoptical characterization of vertical air-gap DBRs, constitutes the new results in this report. The particular structures discussed were grown on free-standing GaN (FS-GaN) substrates to minimize strain, and had a design centre wavelength of 450 nm.

Previous work in this area of microfabrication includes that of Simeonov *et al* who reported a two-step method for removing AlInN sacrificial layers [15]. This involved an initial anodic oxidation step, followed by dissolution of the resulting oxide in a separate process, and was used to fabricate microdisk lasers. In comparison, our wet-etch technique offers greater simplicity. The characterization of these microfabricated air-gap structures presents measurement challenges, particularly in reliable calibration of their reflectivities. Examples of previous measurement approaches are illustrated by work on  $\text{Al}_{0.08}\text{Ga}_{0.92}\text{N}$ -air DBRs made by the PEC method, and grown on buffer layers on sapphire substrates. In an initial report on 3-period DBRs, the average reflectivity in the designed high reflectivity range around 400 nm was reported as being  $4\times$  as high as that from a dry-etched GaN surface, implying an absolute reflectivity in the range 60–72% [5]. Subsequently the same group estimated the peak reflectivity of a 4.5-period DBR from the finesse of a planar microcavity in which it formed one mirror, deriving a value of  $\sim 70\%$  [6].

## Experimental details

Epitaxial GaN-AlInN multilayers were grown in an Aixtron 200/4 RF-S metal organic chemical vapour deposition reactor. Deposition conditions for GaN and AlInN were similar to those in [13], apart from the omission of intentional doping, and the use of FS-GaN rather than sapphire substrates. The FS-GaN substrates were from Lumilog (Vallauris, France), and had

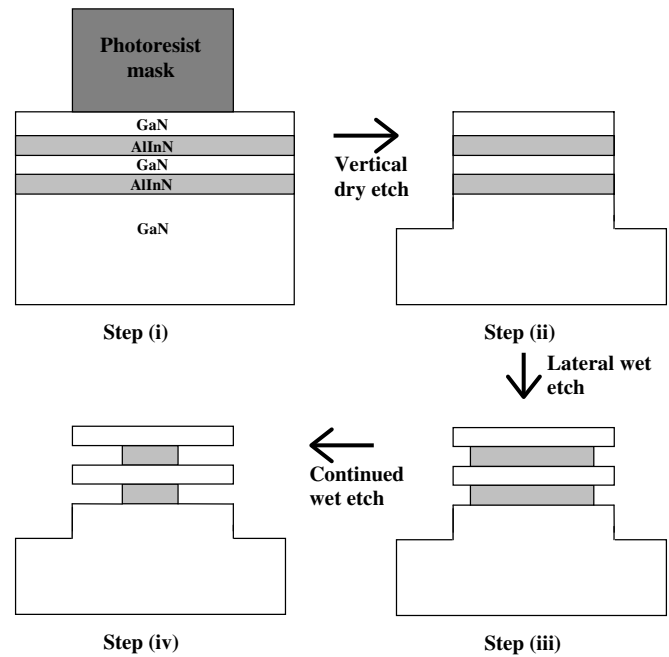


**Figure 1.** Schematic diagram of the process flow for producing the air-gap microstructures. The figure can represent a cross-section either of a cylindrical pillar, or across the width of a microbridge. In the latter case, wet etching can be continued to give complete removal of the AlInN provided that large anchor features are present in front of and behind the plane of the cross-section.

(0001)-orientation and non-polished back surfaces. The design for the GaN-air DBRs used  $\lambda/4$  air layers and  $3\lambda/4$  GaN layers. The corresponding physical thicknesses targeted in growth are tabulated later. All microfabrication steps and measurements were performed on material taken from as close as possible to the wafer centre. The method used to introduce air gaps between GaN layers was similar to that we have reported in [12] and [13], and is illustrated schematically in figure 1. The plan-view form of microstructures was first defined in positive photoresist, corresponding to step (i) in the figure. Next, a Surface Technology Systems model LPX inductively coupled plasma (ICP) tool was used to etch vertically to a depth greater than that of the lowest AlInN layer, using chlorine-argon chemistry. Step (ii) in the figure corresponds to the stage after ICP etching and removal of the residual photoresist mask. The lateral wet etch step to remove sacrificial AlInN layers used aqueous nitric acid of 2 molar concentration, at its boiling temperature. This corresponds to steps (iii) and (iv) in the figure. The nitric acid was heated in a glass reflux apparatus fitted with a water-cooled condenser. The extent of removal of the AlInN is controlled by the duration of the wet etch. The transparency of the III-nitride materials allows the progress to be followed by optical microscope inspection, as illustrated in [12], but residual AlInN also generates contrast observable by scanning electron microscopy (SEM), as shown later in this communication. The range of AlInN lateral etch rates reported in [12] was  $140\text{--}210\text{ nm h}^{-1}$ , and all wet etch steps in the current work were of 14 h duration.

Microreflectivity spectra were recorded using light from a xenon discharge lamp, delivered via  $200\text{ }\mu\text{m}$  fibres to

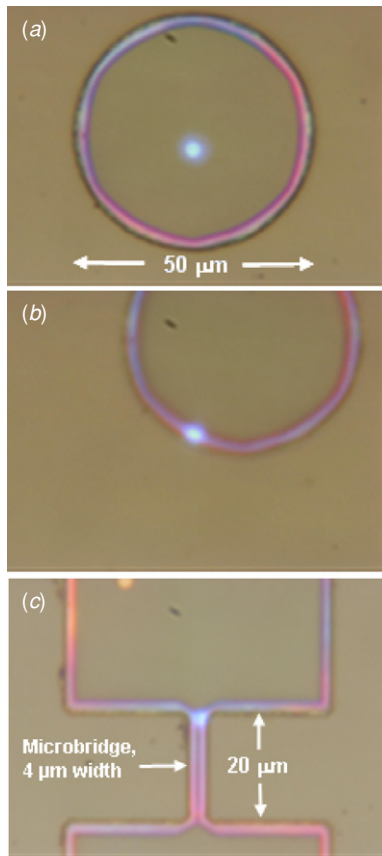


**Figure 2.** Optical micrographs of 3-period microstructures with air gaps. Parts (a) and (b) show a micropillar, while part (c) shows a microbridge with sections of its anchor posts visible at the top and bottom of the image. The bright illuminated spots generated spectra shown in the figure 3 group.

an ultraviolet microscope objective. This had a numerical aperture of 0.5, stopped down using an aperture to  $\sim 0.1$ ; simulations show the resultant  $\pm 6^\circ$  spread of incident angles to have a negligible effect on the reflectivity. The illuminated spot on the samples was  $\sim 4 \mu\text{m}$  in diameter. Detection used an Ocean Optics commercial spectrograph, and reflectivities were calibrated relative to a soda glass reference sample. Real-colour images were also captured. Large-area reflectance spectra of as-grown epistuctures were recorded on a Perkin-Elmer Lambda 2 spectrophotometer. SEM was conducted in an FEI Sirion instrument, without the use of any charge-dissipation coating. Simulations of reflectance spectra assumed normal incidence, and used standard transfer matrix methods [16]. Fitting of simulations to experimental spectra used standard least-squares procedures.

## Results and discussion

The as-grown GaN-AlInN multilayer structures were free from cracks and featureless under optical microscope inspection. Structures with both 2 and 3 sacrificial AlInN layers were grown, but optical characterization is reported only for the latter structures for conciseness. Air-gap structures were prepared in two different geometries, as illustrated in figures 2(a) to (c). Cylindrical pillars etched into the GaN-

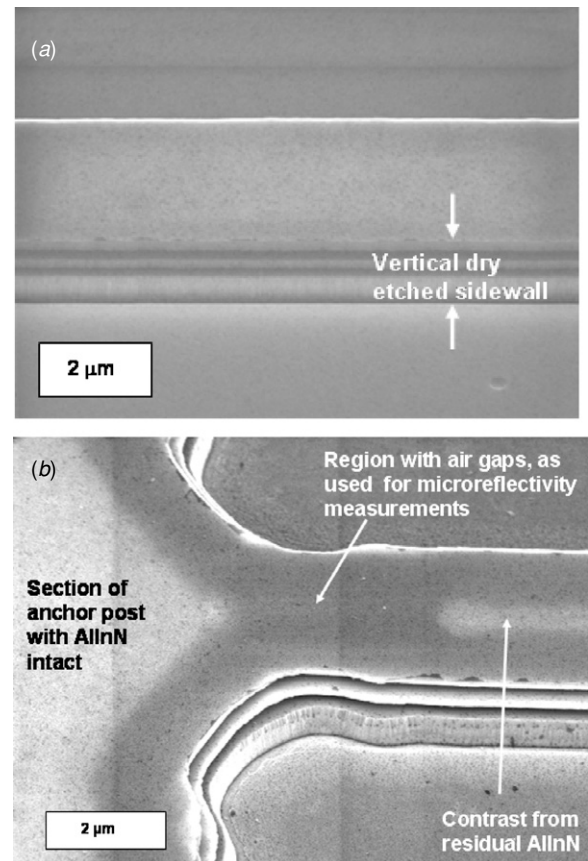


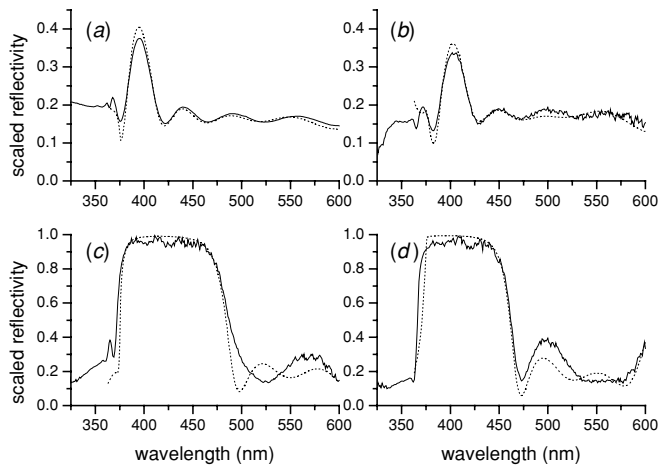
**Figure 3.** Oblique-view SEM images of microbridges fabricated from a 2-period epistucture. Part (a) shows AlInN layers exposed by the dry etch step, which show dark contrast. Part (b) illustrates the introduction of air gaps after the wet etch step.

AlInN multilayers had diameters of  $50 \mu\text{m}$ , and optical microscopy indicated that the wet etch introduced air gaps  $\sim 3 \mu\text{m}$  in width. This extent of lateral etching of the AlInN is consistent with etch rates reported for similar microstructures previously [12]. The second type of microstructure consisted of rectangular beams  $4 \mu\text{m}$  wide by  $20 \mu\text{m}$  in length each supported between two larger square anchor posts. The plan-view geometry was the same as that used to fabricate single-layer doped GaN microbridges for electrical studies reported in [13]. Figure 3(a) shows an oblique SEM image of a microstructure containing two AlInN layers, which have been exposed by vertical ICP etching, but not yet subjected to wet etching. This processing stage corresponds to step (ii) in figure 1. The layer thickness uniformity and the flatness of the GaN top surface are evident. Figure 3(b) illustrates a similar microstructure after wet etching, and shows contrast indicating areas where AlInN remained in place. Microbridges in this state proved advantageous to microreflectivity studies, because the mechanical pinning by the residual AlInN prevented any flexure of the GaN layers under residual stress.

The significant refractive index difference between GaN and lattice-matched AlInN gave rise to pronounced maxima in the reflectance spectra of the as-grown multilayers. This feature is illustrated by the large-area reflectance spectrum from a 3-period GaN-AlInN structure shown in figure 4(a), showing a peak at 399 nm. Simulations

**Table 1.** Summary of layer thicknesses, repeat periods, and scaling factors from simulations of reflectance spectra, compared with the nominal designed values in the left-hand column.

	Target thicknesses in growth	Fitted parameters as-grown epistucture	Fitted parameters centre of micropillar	Fitted parameters edge of micropillar	Fitted parameters microbridge
GaN thickness (nm)	136	122	131	117	113
AlInN thickness (nm)	113	121	116	–	–
Air thickness (nm)	–	–	–	132	115
Period (nm)	249	243	247	249	228
Scaling factor for fitting	–	1.04	1.08	1.52	1.35

**Figure 4.** Scaled experimental reflectance spectra (solid lines) and simulations (dashed lines) for various 3-period structures: (a) macro-scale area of as-grown epistucture, (b) centre of a wet-etched micropillar, (c) air-gap region at the edge of a wet-etched micropillar, (d) 'pinned' air-gap region at the end of a wet-etched microbridge.

of spectra assumed dispersion relations for the III-nitride materials of the form described in [17], i.e.  $n^2(h\nu) = C + Ay^{-2}(2 - (1+y)^{\frac{1}{2}} - (1-y)^{\frac{1}{2}})$ , where  $y = h\nu/E_g$ ,  $E_g$  is the effective bandgap, and  $C$  and  $A$  are dimensionless parameters. For GaN, the required parameters were  $E_g = 3.42$  eV,  $C = 2.66$ , and  $A = 9.98$ , while for lattice-matched AlInN values of  $E_g = 4.34$  eV,  $C = 1.65$ , and  $A = 12.13$  were used, following [7]. Except where noted, the simulations used the realistic constraint of equal thicknesses for each equivalent layer (i.e. a periodic structure). Table 1 compares the best-fit thicknesses for the GaN and AlInN layers and the corresponding repeat period, with the values targeted in growth. Also tabulated is a scaling factor, which is the constant by which the experimental reflectance values must be multiplied to optimize the fit to the simulated spectrum. As expected in a situation where measurement of near-absolute reflectance values is straightforward, the scaling factor is close to unity (1.04) for figure 4(a). The spectral region on the short-wavelength side of the main reflectivity peak coincides with the band edge region of GaN, corresponding to the room-temperature bandgap of 3.42 eV. Short-period oscillations of excitonic origin are present in the experimental spectrum, and the minimum at 376 nm is reproduced in the simulation.

Microreflectivity measurements were also made on the central regions of cylindrical micropillars unaffected by

the wet etch. Figure 2(a) shows the illuminated area corresponding to the spectrum in figure 4(b). The similarity in form of the spectra in figures 4(b) and (a) is obvious. Table 1 shows a best-fit GaN layer thickness from simulation of figure 4(b) is  $\sim 4\%$  smaller than the target value in growth, while the best-fit AlInN thickness is  $\sim 3\%$  larger than the target value. The scaling factor for optimized fitting is now 1.08. In this case, the microstructure analysed was laterally uniform over dimensions much larger than the measurement spot. Comparison of the large-area and micro-reflectivity measurements from these and other similar structures demonstrates a small increase in the scaling factor for the system including the microscope objective. The authors of [5] also commented on this issue.

Next we consider microreflectivity spectra from the air-gap regions at the edges of micropillars. The illuminated area shown in figure 2(b) produced the spectrum shown in figure 4(c). An obvious new feature is the extended wavelength range over which high-reflectivity values were observed, and the reflectivity exceeds 90% of the noise-averaged maximum value over 87 nm. The centre of the stopband, defined as the wavelength midway between the two 90% positions, is at 423 nm. The scaling factor required to optimize the fit of the simulated spectrum with the experimental spectrum is 1.52. The measurement spot was known to be slightly larger than the width of the air-gap region, which can account for the further increase in the scaling factor from the case of the pillar centre. Also any strain gradients present within the GaN layers could potentially compromise the assumption of parallelism, and such effects are very challenging to observe by SEM. Thinning of the GaN layers via parasitic attack by the wet etch used to remove the AlInN layers could also lead to thickness variations in the completed air-gap structure, since GaN at the outermost edge of the pillars was exposed to the wet etch longest. Previously observed trends in the polarity dependence of GaN etching suggest that thinning would occur largely on the  $(000\bar{1})$  face, corresponding to the underside of the GaN layers. Our estimate of the magnitude of any such parasitic etch effect in [14] suggests that the maximum GaN thickness loss should be  $\sim 5$  nm. However, the best-fit layer thicknesses summarized in table 1 are consistent with rather larger (14–19 nm) reductions in the average GaN layer thickness, with a corresponding increase in the air-gap thickness from the starting thickness of the AlInN layers. To explore the possible influence of generalized geometrical perturbations, a spectrum simulation was performed with the periodicity constraint removed. Layer thicknesses from the

top surface were fitted to the following values: GaN 111 nm, air 118 nm, GaN 122 nm, air 112 nm, GaN 126 nm, air 113 nm. Assumption of this aperiodic structure allowed better fitting of the secondary reflectance peak at  $\sim 575$  nm (data not shown), but with no improvement in the scaling factor.

Finally, we discuss the optical characterization of wet-etched microbridges, where we concentrated on measuring the ends of bridges as shown in figure 3(b). An optical micrograph of one such illuminated area from a 3-period structure was shown in figure 2(c), and the corresponding reflectivity spectrum is presented in figure 4(d). The experimental spectrum shows a high-reflectivity stopband of similar width to that in the spectrum from the wet-etched micropillar. The required scaling factor is now 1.35 and the average measured reflectivity was  $\sim 70\%$ . Once again the reduction in measured reflectivity compared to the simulation can be related to the size of the measurement spot relative to the area of a uniform air-gap region, as seen in figure 2(c). The reflectivity exceeds 90% of the maximum value over a wavelength range of 73 nm. The centre of the stopband, defined as above, is now at 409 nm. The overall blueshift of this spectrum relative to that air-gap structure previously discussed has a consequence that the secondary excitonic maximum at 368 nm seen in figure 4(c) is no longer resolved. Consistent with this blueshift, the simulated period of the GaN-air structure is now significantly lower than in the previous case. The ratio of the fitted GaN and air-layer thickness is also significantly different from the case of the micropillar structure, and the fitted air gap thickness is within 2% of the designed AlInN thickness. These observations do not support pronounced thinning of the GaN layers by the wet etch, which would be manifest by thicker air-gap layers. Furthermore, the fitted combination of GaN and air-layer thickness agrees qualitatively with the expectation for material away from the exact wafer centre; GaN growth rates decrease with increasing distance from the wafer centre, while AlInN growth rates remain relatively constant.

## Summary and conclusions

This work has shown the feasibility of fabricating GaN/air vertical DBRs by the use of multiple sacrificial AlInN layers, which were removed by etching in hot nitric acid. Microstructures designed for peak reflectivity at 450 nm, and comprising 2 or 3 repeat periods of  $3\lambda/4$  GaN layers and  $\lambda/4$  air-gap layers, proved mechanically robust. Micro-optical characterization indicated strikingly wide high-reflectivity stopbands, consistent with simulations based on the idealized geometries. Using a criterion of the positions of 90% of the maximum reflectivity, stopband widths as large as 87 nm were demonstrated for a 3-period DBR. Such structures showed peak reflectivities of  $>70\%$ , matching the best results reported from a more elaborate photoelectrochemical fabrication method [5, 6]. Our reflectance values are most likely limited by the small scale of the features in comparison with the measurement spot. The spectrum simulation technique offers insight into effects such as parasitic etching of the GaN layers during removal of the AlInN layers, but the balance of available evidence already suggests this effect is

not severe. Air-gap DBRs fabricated by the route described could be developed further to feature electrostatic tuning, and/or be integrated with active emitters (e.g. to form resonant cavity light-emitting diodes) and microcavities. Also wider applications of the sacrificial layer technology are expected in fabrication of microelectromechanical sensors and actuators [4, 13].

*Note added in proof.* The authors wish to note an independent publication on GaN/air vertical DBRs published shortly after submission of our own manuscript (Altoukhov A, Levrat J, Feltin E, Carlin J-F, Castiglia A, Butté R, Grandjean N 2009 *Appl. Phys. Lett.* **95** 191102). This work used a two-step method for removal of AlInN sacrificial layers, as originally reported in [15] of our own paper.

## Acknowledgments

We acknowledge the EU FET-Open Program STIMSCAT FP6-517769 and the EPSRC grant EP/D078555/1 for financial support, including funding of the microfabrication work conducted by C Xiong at the Institute of Photonics.

## References

- [1] Streubel K, Rapp S, André J and Chitica N 1997 *Mater. Sci. Eng. B* **44** 364
- [2] Sagnes I, Strassner M, Bouchoule S, Leclercq J-L, Regreny P, Bakouboula A, Rienenschneider F and Meissner P 2004 *C. R. Phys.* **4** 675
- [3] Hasse A, Irmer S, Daleiden J, Dharmarasu N, Hansmann S and Hillmer H 2006 *Electron. Lett.* **42** 974
- [4] Cimalla R, Pezholdt J and Ambacher O 2007 *J. Phys. D: Appl. Phys.* **40** 6386
- [5] Sharma R, Haberer E, Meier C, Hu E L and Nakamura S 2005 *Appl. Phys. Lett.* **87** 051107
- [6] Sharma R, Choi Y-S, Wang C-F, David A, Weisbuch C, Nakamura S and Hu E L 2007 *Appl. Phys. Lett.* **91** 211108
- [7] Carlin J-F, Zellweger C, Dorsaz J, Nicolay S, Christmann G, Feltin E, Butté R and Grandjean N 2005 *Phys. Status Solidi b* **242** 2326
- [8] Watson I M, Liu C, Gu E, Dawson M D, Edwards P R and Martin R W 2005 *Appl. Phys. Lett.* **87** 151901
- [9] Butté R *et al* 2007 *J. Phys. D: Appl. Phys.* **40** 6328
- [10] Cho E, Pavlidis D and Sillero E 2007 *Phys. Status Solidi c* **4** 2767
- [11] Rizzi F, Edwards P R, Bejtka K, Semond F, Kang X N, Zhang G Y, Gu E, Dawson M D, Watson I M and Martin R W 2007 *Appl. Phys. Lett.* **90** 111112
- [12] Watson I M, Xiong C, Gu E, Dawson M D, Rizzi F, Bejtka K, Edwards P R and Martin R W 2008 *Proc. SPIE* **6993** 69930E
- [13] Xiong C, Massoubre D, Gu E, Dawson M D and Watson I M 2009 *Appl. Phys. A* **96** 495
- [14] Xiong C, Rizzi F, Bejtka K, Edwards P R, Gu E, Dawson M D, Martin R W and Watson I M 2010 *Superlattices Microstruct.* **47** 129
- [15] Simeonov D, Feltin E, Altoukhov A, Castiglia A, Carlin J-F, Butté R and Grandjean N 2008 *Appl. Phys. Lett.* **92** 171102
- [16] Hecht E and Zajak A 1987 *Optics* 2nd edn (New York: Addison-Wesley)
- [17] Brunner G, Angerer H, Bustarret E, Freudenberg F, Hopler R, Dimitrov R, Ambacher O and Stutzmann M 1997 *J. Appl. Phys.* **82** 5090